Numerical and Experimental Analysis of Multichannel Analysis of Surface Waves Test for Detection of Underground Voids

Hassan Ali & Giovanni Cascante
University of Waterloo, Waterloo, ON, Canada

ABSTRACT
The identification of underground voids is very important for any geotechnical site investigation. Geophysical methods are commonly used to locate the underground voids; but limitations need to be addressed. For example, the effect of lateral in-homogeneities in the surface waves test is not well understood. In this paper, multi-channel analysis of surface wave (MASW) method is used for the detection of underground cavities using the numerical and experimental analysis. The experimental test is conducted on a sandbox having a known void. Different signal processing techniques such as dispersion curves, frequency-spectra contour plots, and two-dimensional Fourier transform are used for the data analysis. A new methodology is adopted where the total seismic array of receivers is divided into three sections: before, on-top, and after the void. Results from a numerical model developed in the FLAC 2D is used to compare the results with experimental data. Results show that the void induces vibration amplifications at the surface in front of its location, i.e. before void; however, shows attenuation in surface responses after the void. These effects are observed when the void is located within the one-third of the wavelength. Numerical and experimental results show that the results of the MASW test and the advance signal processing techniques can be successfully used in the identification of the underground voids.

RÉSUMÉ
L'identification des cavités souterraines est très importante pour toute étude de géotechnique. Les méthodes de géophysiques sont couramment utilisées pour localiser les cavités souterraines, mais des limitations doivent être posées. Par exemple , l'effet des inhomogénéités latérales dans le test des ondes de surface n'est pas bien comprise . Dans cet article, l'analyse multi-canal des ondes de surface: la méthode (MASW) est utilisée pour la détection des cavités souterraines en utilisant des analyses numériques et expérimentales. Le test expérimental est mené sur un bac à sable, à l'intérieur duquel se trouve une cavité artificielle prédéfinie. Des différentes techniques de traitement du signal, telles que les courbes de dispersion, le tracés des contours du spectre fréquentiel , et la transformée de Fourier à deux dimensions sont utilisés pour l'analyse des données. Une nouvelle méthodologie est adoptée lorsque le réseau sismique total de récepteurs est divisé en trois sections: avant , au-dessus , et après la cavité. Un modèle numérique a été développé avec le logiciel FLAC 2D pour comparer les résultats avec les données expérimentales. Les résultats montrent que la cavité entraine une amplification des vibrations à la surface en face de son emplacement , c'est à dire avant la cavité, mais une atténuation dans les réponses de la surface après le vide. Ces effets sont observés lorsque la cavité est située dans le tiers de la longueur d'onde . Les résultats numériques et expérimentaux montrent que les résultats de l'essai MASW et les techniques poussées de traitement du signal peuvent être utilisés avec succès dans l'identification des cavités souterraines.

1 INTRODUCTION

For any geotechnical site characterization, location of soft sedimentary soil layer, shallow bedrock, and detection of underground anomalies is very important. This information is critical for the design of foundations, embankments, tunnels, and seismic design of civil infrastructures. Among the various methods available for the site characterization, the use of the non-invasive geophysical techniques is a valuable tool in any design process.

In spite of improvement in the geophysical methods, identification of sub-surface ground anomalies is still a challenging problem. Ground-penetrating radar has been successfully implemented for shallow depths; yet, problem arises when the underground surface consists of high conductivity materials such as clays (Kong et al., 1994). Seismic reflection can be used to locate underground cavities in the presence of horizontal soil layers above and below the void.

Multi-channel analysis of surface waves (MASW) is a geophysical technique that has gained attention and acceptance for the detection of underground voids (Nasseri-Moghaddam et al., 2007). The MASW technique uses Rayleigh waves for estimating the soil stiffness profile at a site. Due to the scattering of the Rayleigh waves by the heterogeneities, analytical description is difficult and therefore field experiments and numerical models are carried out to study this problem. Phillips et al. (2004) conducted field tests, experiments on prototypes, and numerical studies and reported areas of high-energy concentrations on the surface response over different voids. Similarly, various numerical models with the lateral inhomogeneities showed that the presence of an anomaly causes rippled signals in the time domain. These ripples are more noticeable in the area between the source and the void, because part of the incident wave energy is reflected back from the void. It was further mentioned that the width of the void affects the pattern of ripples while embedment depth of void affects the amplitude of the reflections. In general, these studies show a good agreement between the numerical simulation and the experimental results.

In order to study the effect of void size and location different studies are carried out to associate the surface response of a medium to the location and size of void. Philips et al. (2001) performed field and laboratory

experiment tests and presented the results in the frequency domain. They reported regions of high energy concentrations in the vicinity of the void and hence suggested the use of power spectral density functions (PSD method) for the detection of the voids. Shokouhi and Gucunski (2003) used wavelet analysis of the surface responses to correlate the width of the high-energy region to the size of the void. Methods discussed above do not consider the embedment depth of the void and are based on the changes of the surface responses. Recently Nasseri-Moghaddam et al. (2007) developed techniques that are useful in locating the void and estimating its embedment depth. However, the application of the MASW method for void detection is usually limited to shallow depths, mostly due to difficulties of generating long wavelengths with high signal-to-noise ratios, and partly because of the lack of understanding of the interaction of the embedded voids and the Rayleigh waves. In general, these studies show a good agreement between numerical simulation and experimental results.

In this paper, the effect of underground void on dispersion curves obtained from numerical models simulating MASW test in the presence of lateral homogeneities are studied. The objective of this research is to provide define strategies for the selection of optimal MASW test configuration for the detection of voids for a given site condition. Numerical data from two dimensional (2D) axis-symmetric models for this study are acquired from Moghaddam (2006). The model comprises of voids having variable width and embedment depth. To understand the influence of array length on underground void; the total surface recording points of the numerical model are divided into three sections: before, ontop, and after void. Surface responses from these sections are analysed in the time and frequency domain. The 2D-FFT or Frquency-wavnumber (f-k) plots for each model are developed using computer software package SWAN. The f-k plots not only indicate the velocity of the wave propagating but also indicates the energy density within a given time interval. Dispersion curves are calculated using 2D-FFT data from SWAN. These dispersion curves are further evaluated to identify general pattern between the no-void and void cases.

2 THE MASW TEST METHOD

The multi-channel analysis of surface wave (MASW) is a non-destructive technique used for evaluation of shear wave velocity profile. MASW is an extension of SASW method based on the work by Nazarian et al. (1984). It utilizes several transducers for computation of underground responses. The approach of using several transducers effectively allow the removal of noise and help in identification of higher order Rayleigh wave modes (Park et al., 1999). As Rayleigh waves are confined to the near surface of the ground, therefore low energy seismic source is usually recommended for lab and field tests.

Rayleigh waves are dispersive in nature and dispersion of the Rayleigh waves are used in the evaluation of the sub-surface stiffness profiles. Since the stiffness of the soil usually increases with the depth, the depth to which the Rayleigh wave causes significant displacement increases with increasing the wavelength. Low frequency (long wavelength) propagates faster than high frequency (short wavelength). Thus it can be concluded that penetration depth of Rayleigh wave is inversely proportional to its frequency. Usually, maximum penetration depth is considered to be one wavelength in field and laboratory. Frequency spectra and dispersion curve (phase velocity profile) for a site are obtained from the time domain signals. These dispersion curves can be inverted to estimate the shear-modulus profile of the medium (Stoke et al., 1988).

For low energy seismic sources, sledgehammer is commonly used in the industry. Mechanical harmonic sources and passive sources such as ambient noise and micro-tremors have also been used. The source should be able to yield enough energy over the required test frequency range to allow the detection of Rayleigh waves above background noise. Velocity transducers (geophones) are used to collect the surface responses in the low frequency range (4 Hz to 100 Hz); whereas, accelerometers are used for higher frequencies (100 Hz to 5000 Hz) (Cascante et al., 2006). The distance between the source and first receiver determines the largest reliable wavelength in the measurements. On the other hand, the distance between the transducers and the sampling rate determine the smallest reliable wavelength. A common practice is to choose a source to receiver distance equal to at least twice the maximum required wavelength (Hiltunen and Woods, 1989).

3 NUMERICAL SIMULATIONS

3.1 Numerical model setup

In order to study the effect of the void width and size on the surface waves responses; the surface response data was obtained from Nasseri-Moghaddam (2006). This section provides the details of the finite difference program FLAC (Itasca, 2000) used for the numerical simulations. In the MASW tests, the medium properties and the propagation pulse governs the wave propagation through the medium. The medium properties include the modulus of elasticity E, the Poisson ratio ν, the mass densityρ, and the material damping D. Since material damping is small for low strains and independent of frequency (Santamarina et al., 2001), material damping is ignored. The selected material properties for the numerical model are presented in Table 1.

Table 1: Numerical model medium properties

Density	ρ	1600 kg/m^3
Young's Modulus	E	19 MPa
Poisson's Ratio	ν	0.2
Compression Wave Velocity	V_P	114.9 m/sec
Shear Wave Velocity	V_S	70.3 m/sec
Rayleigh Wave Velocity	V_R	64.08 m/sec

Figure 1 illustrates a general sketch of the two-dimensional axisymmetric model used for the simulations. Figure 1a shows the location and embedment depth of the void, while Figure 1b presents the configuration of array sections. Model parameters are adjusted to match

theoretical results and to verify that the model accurately predicts the R-wave propagation in a semi-infinite medium. The model consists of a central uniform grid surrounded by a non-uniform grid.

The axis of the symmetry is defined at the left end boundary, while quiet boundaries are defined at the right and bottom. To effectively reduce the reflections of R-waves, the boundaries of the numerical model are practically positioned as far from the void as possible. The distance between the receivers and boundary is selected in a manner to ensure that the reflections from the boundary are greater than the main Rayleigh wave arrival at any receivers. Reflections from the R-wave generated after the interaction of the main R-wave event with the void are practically not affected by boundary reflections because of their geometrical attenuation. The sampling frequency is f = 100 kHz (time increment $\Delta t = 10^{-4}$ s). Lamb source f (t) presented in Equation 1 is applied to the numerical simulations (Lamb, 1904). The forcing function is applied to the left boundary.

$$f(t) = \frac{F_b}{\pi} \frac{\tau}{t^2 + \tau^2} \qquad [1]$$

In Equation 1, F_b and τ are the constants that modify the amplitude and the frequency content of the forcing function respectively.

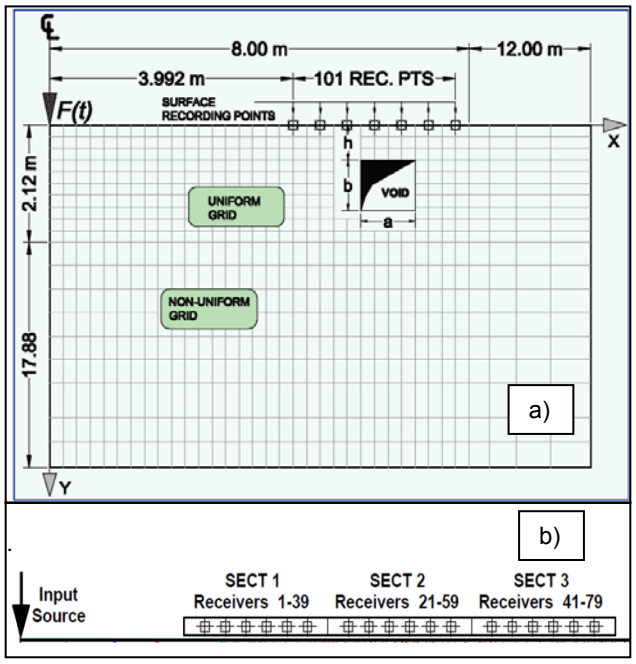

Figure 1: Configuration of the basic finite difference model. a) Numerical model showing the distances of the recording points and source. b) Configuration of receivers in sections.

3.2 Methodology

Rectangular voids of variable width, height, and embedment depth were studied; however, in this paper the results for void having size 0.08 m in depth, width, and height are presented. Details of the analysis of the other models can be found under Ali et al. (2011) and Nasseri-Moghaddam (2006). Surface responses are recorded from a total of 101 recording points. The maximum and minimum reliable wavelengths considered for the model are λ_{max}= 2.0 m (f = 32 Hz) and λ_{min} = 0.08m (f = 801 Hz), respectively. In order to reduce near-field effects, recording points are located far from the source.

A new methodology is adapted in this paper to divide the total array of receivers into three sections: section 1 (1-39) defines array of recording points before void, section 2 (21-59) centered on the void, while section 3 (41-79) after the void, respectively. The length of the array in each section is kept constant, i.e., 38 receivers. Further, the calibration of the numerical model is performed by changing the model parameters such that the responses measured from numerical model without void matches well with the theoretical model. Details of calibration can be found in (Nasseri-Moghaddam, 2006).

3.3 Analysis of results in time domain

Figure 2, shows the typical time traces of surface responses, due to the Rayleigh waves, for section 1, 2, and 3. The time window in the figure is selected in such a way to demonstrate the main features of the R-waves; since the amplitude of other waves is negligible as compared to the R-waves. The solid line represents surface response in the presence of the void while dash line represents surface response from the no-void case. In each of the three sections, the arrival of main pulse can be seen. Effect of reflections from void can be clearly observed in sections 1 and 2.

3.4 Analysis of results in frequency domain

Figure 3 shows a comparison of the typical Fourier spectra of the vertical displacements obtained from time traces in Figure 3. Fourier spectra is shown for the no-void (dash line) and the void (solid line) cases. The amplitudes of the spectra are normalized based on the section having lowest amplitude. Therefore, the spectra are normalized based on the section 3. A Fourier spectrum of the no-void case is relatively smooth in all the three sections. The minor undulations shown in section 1 can be attributed to the reflection of P-waves from the model boundaries.

3.5 Frequency-wavenumber f-k (2D FFT) analysis

In this study a commercial software package SWAN (Geostudi Astier, 2010) is utilized for processing of the data. The surface responses from each model are processed in SWAN to obtain frequency-wavenumber (f-k) plots. Typical f-k plot for no-void and void cases are shown in Figure 5. The contours represent energy amplitude. Observing the spectrum, it can be seen that, the main part of energy (dark blue and cyan color) in this case is between 50 and 100 m/sec. For the evaluation of experimental dispersion curve, these areas of energy concentrations should be searched for local maxima of

the spectrum's amplitude. Each line exiting from the FK spectrum represents velocity. Using f-k plots the direction and apparent velocity of seismic waves can be examined. Thus the slope of a frequency-wavenumber plot is related to the speed of propagation of wave. The wave number range represents the direction of traveling wave, i.e., positive wavenumber shows waves propagating in the forward direction (away from the source), and vice versa. In the Figure, Rayleigh and P-waves can be identified using the slope of f-k plot. The values plotted in Figure 5 are logarithmic values.

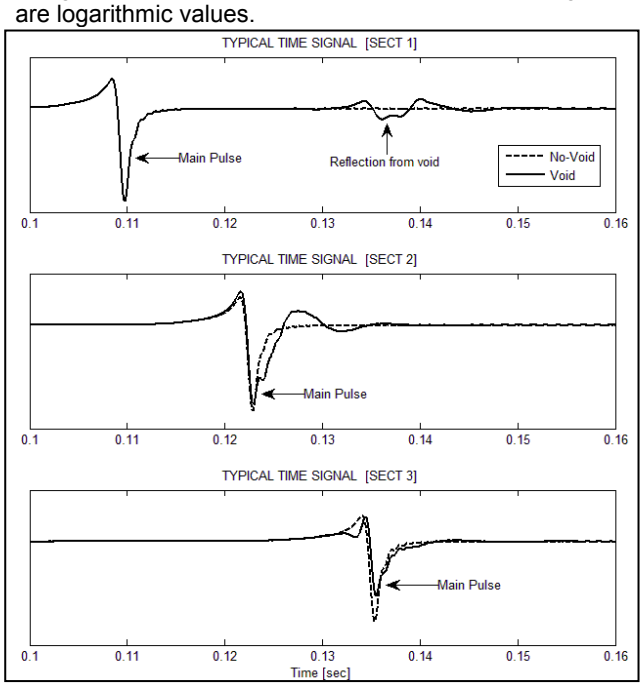

Figure 2: Time responses of section 1, 2, and 3.

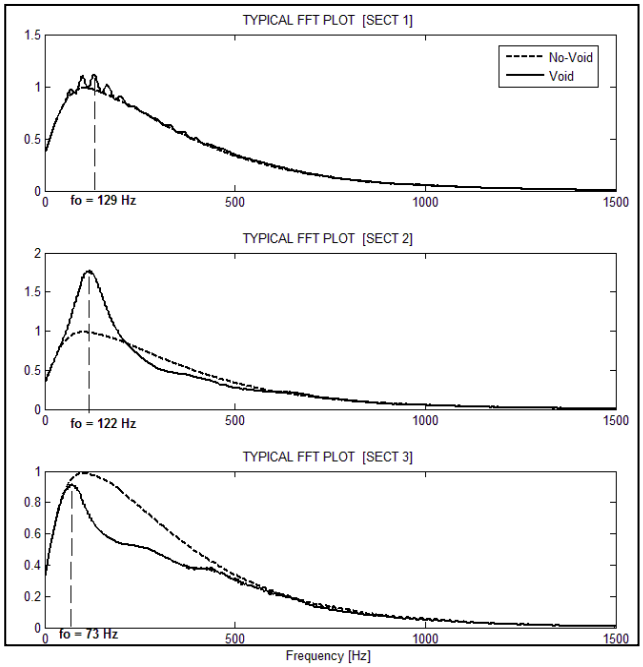

Figure 3: Fourier Transform of section 1, 2, and 3.

3.6 Dispersion curves

A dispersion curve describes the variation in the velocity with frequency. Figure 6 shows typical dispersion curves for section 1, 2, and 3 obtained using SWAN for time traces presented in Figure 3. Similar to previous results, comparison have been made between no-void and void case for each section. Solid line in Figure 6 represents data with the void, while dash line represents data with the no-void model. Dashed horizontal line in each section shows the R-wave velocity. These dispersion curves are obtained by selecting the local maxima from the f-k spectrum. Dispersion curves obtained from the SWAN are smoothed using a Gaussian function having a bandwidth of 10.

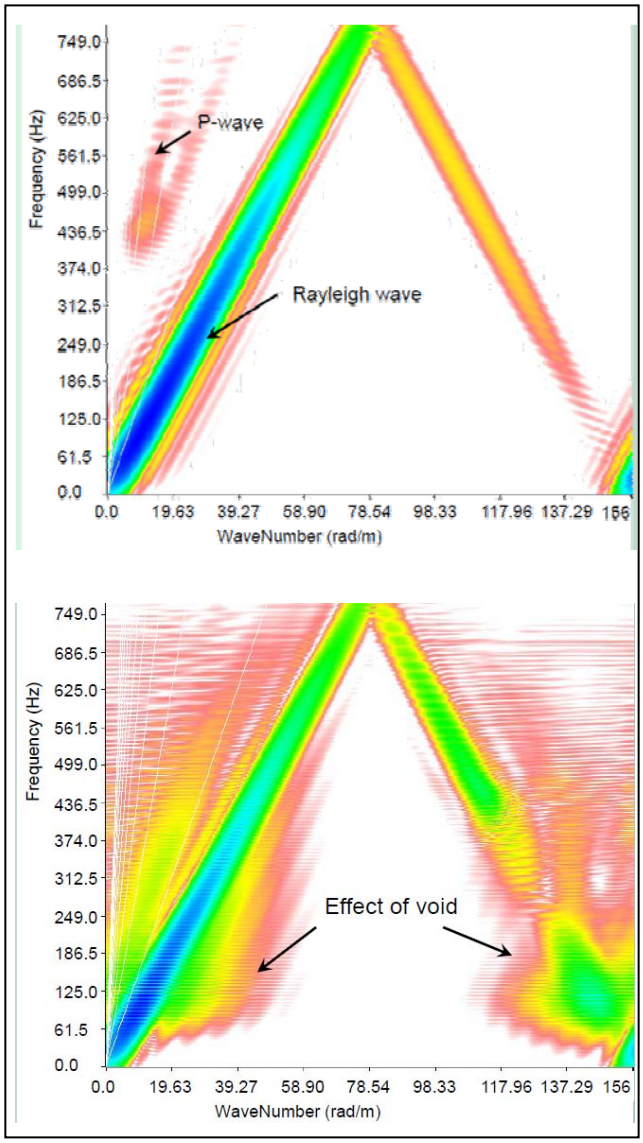

Figure 4: Frequency-wave number (2D-FFT) plots. Effect of void can be seen along with the frequency range

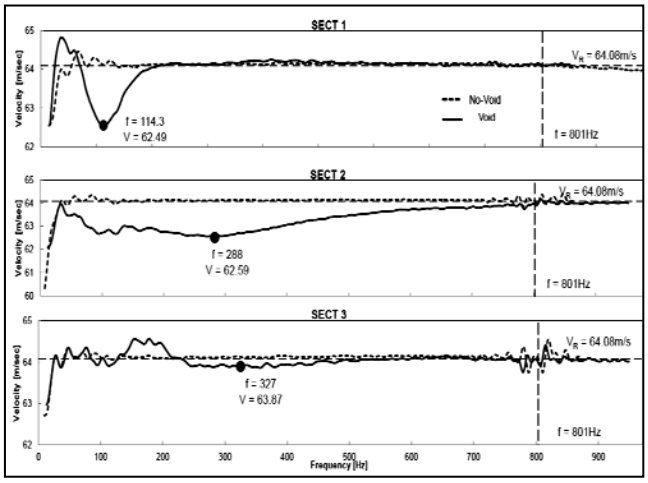

Figure 5: Dispersion Curves of section 1, 2, and 3

3.7 Pattern identification and normalized wavelength (λ)

Once the dispersion curves were obtained, the next step was to identify the pattern between sections for each model. The pattern identification was based on the trend (change) in frequency for dispersion curves having void and comparing them with the no-void case. This method would ensure that the change in velocity is due to the effect of the void and not a numerical model error. Figure 5 illustrates this identification of pattern by circular markers on the dispersion curves. Velocity and frequency values are also noted for the identified points. These values are summarized in Table 2.

To understand the effect of void size on dispersion curve as a function of wavelength; wavelength (λ) is calculated for each section based on the identified pattern. Wavelength is evaluated using the expression

$$\lambda = \frac{V_R}{f} \qquad [2]$$

In the above equation, V_R is the Rayleigh wave velocity (64.08 m/s) and f is frequency obtained from pattern identification. Finally, the normalized wavelength values are obtained using the relation:

$$\lambda_{norm} = \frac{\lambda}{H} \qquad [3]$$

where H is the sum of the void height and the embedment depth of void, i.e., (H = a + h).

Table 2: Pattern identified frequency and velocity

	Freq [Hz]	**Vel**	**λ**	**λ_{norm}**
Section 1	114.3	62.49	0.56	3.50
Section 2	288.1	62.59	0.22	1.38
Section 3	327.1	63.87	0.20	1.25

3.8 DISCUSSION

From the time traces, it can be observed that the presence of the void has considerable effect. Due to the interaction of the incident Rayleigh wave and near boundary of the void, part of the energy is reflected back in the form of R-waves; this can be observed in section 1 marked as reflection from void.

In a homogenous medium the Fourier spectra for the no-void model are smooth and its shape does not change with the distance, however the amplitude decreases. Maximum energy occurs at a frequency of about 100Hz, which corresponds to a wavelength of 0.6408m ($\lambda = V_R/f$). In this case the Fourier spectra are not smooth and different shapes of the spectra indicates that the medium is dispersive. The values at which maximum energy occurs for the void case are shown in Figure 3. Higher amplitudes are observed at section over the void and attenuation is observed in section after the void. The results of amplitude variation show that in the presence of void not only energy concentration occurs but also the attenuation happens in the frequency ranges 50 – 350 Hz.

From the results shown in Figure 4, the linearity of Rayleigh and P-waves show that there is no numerical dispersion for the frequency-wavenumber range mentioned. From the values of wavelength obtained from pattern identification, λ values increases as the embedment depth of the void increases and frequency decrease, i.e., considering the case of section 1, the frequency values are f = 114.3, while the calculated λ value is $\lambda = 0.56$. This trend shows that as the wavelength increases, frequency decreases for a constant velocity. Comparison of λ_{norm} within sections show that section1 follow 1/3rd rule, i.e., the velocity with which each frequency propagates represents the properties of the material that lies about one third of the wavelength. However, this trend is not shown by values in the sections 2 and 3.

4 EXPERIMENTAL TESTING

4.1 Laboratory test setup

For this study, the physical system to be modeled is a laboratory sandbox. The sandbox, with overall dimensions of 1.06 x 0.87 x .83 (length, width, and height) meters, was filled in two layers. The bottom layer 0.55 meters in thickness consists of dry sand, while, top layer 0.23 meters in thickness consists of cemented sand. A semi-elliptical underground void (0.15 meters width and 0.10 m height) is placed 0.08m from top. To minimize reflections from sandbox boundaries, Styrofoam was placed on the inside walls and floor of the sandbox. From the medium properties of material, the measured Rayleigh wave velocity for the cemented sand is 1000 m/sec and 240 m/sec for dry sand. Figure 6 shows the sectional view of the sandbox and layout of receivers for the two lines of test.

The seismic source was a shaker type sinusoidal pulse. To transmit maximum energy to the sandbox a metal bar (1cm x 1cm) with a metal and plastic tip at one end is fixed to the shaker metal base. Twenty four

accelerometers with a linear frequency response from 10Hz to 10kHz are used to measure surface responses. The surface responses are recorded with a 24-channel data acquisition system at a sampling rate of 100 kHz.

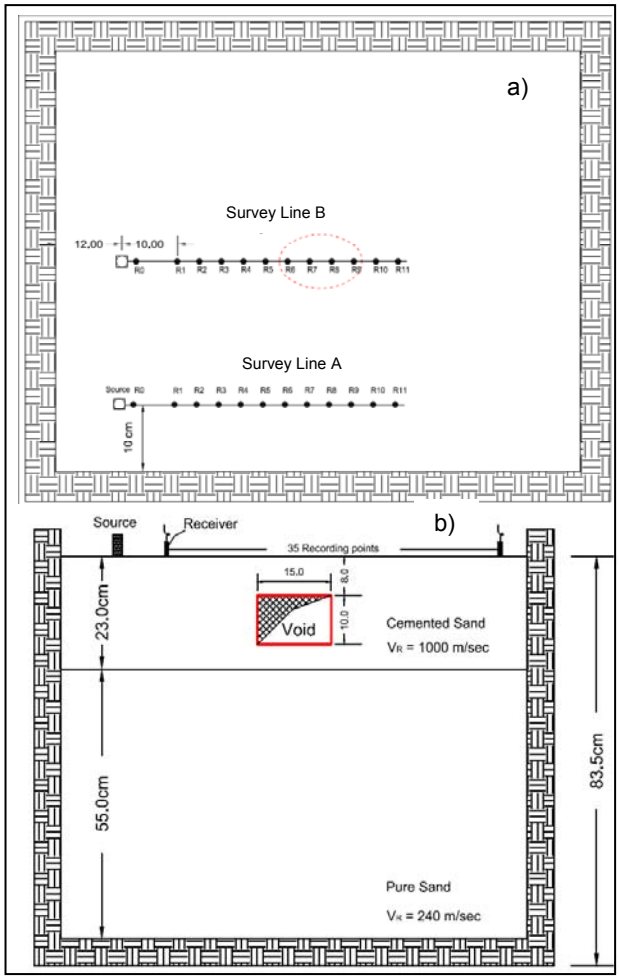

Figure 6: Sandbox test configuration. a) Survey lines with source distance and b) sectional view of sandbox

The surface responses from the sandbox are surveyed along two lines parallel to each other and along the longest dimension of the sandbox as shown in Figure 6. Line B is located on the centerline of the sandbox directly above the void; while, line A is located between the void and boundary of the sandbox. Total length of the survey line is 0.44 m with 11 receivers spaced four centimeters apart. The distance from the source to first receiver is 0.12m. A total of four measurements were collected and average time signals for each receiver are obtained. Results from one accelerometer glued closed to the source was analyzed in time and frequency domains to study the impact of source and frequency generated from metal and plastic tips. Figure 7 shows the frequency spectra for the metal and the plastic tips. Also shown are the average frequency spectra from the receivers. Based on these results, metal tip was used for the experimental testing as it provides a wide range of input energy for the source.

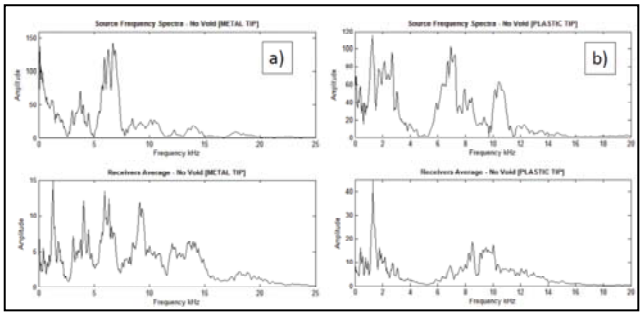

Figure 7: Frequency spectra for source and receivers (average). a) Metal tip and b) Plastic tip

4.2 Results laboratory test

Figure 8 and 9 shows the time traces and the frequency spectra for the no-void and the void cases. Events corresponding to the R-wave are shown. The velocity evaluated from the Rayleigh wave is approximately equal to V_R = 1212 m/sec, the value matches with the value reported for cemented sand (Yang, 2009). Figure 9 is normalized to the maximum amplitude (in this analysis for void case). In plot 'b' of the Figure 9 the void boundaries are shown as dashed lines. Energy concentration can be seen on the top and in the vicinity of the void. A strong reflection from the near boundary of the void can be seen on trace no. 5. Attenuation can be seen after the void which shows that the void reflects and attenuates frequencies in the range of 4 – 10 kHz. The amplitudes of the spectrum on survey line B is 10% higher than the amplitudes on survey line A. Vibrations from sandbox boundaries are also shown on the plot. These reflections are not visible in void case as the survey line is far from sandbox boundaries.

Two-dimensional FFT analysis using SWAN was carried out on laboratory test results as shown in Figure 10. The solid line corresponds to the phase-velocities. The phase-velocities for the no-void case are between 800 and 1600 m/sec, while in the case of the void the phase-velocities are between 700 and 1700 m/sec. The maximum spectral energy occurs between 5.7 and 6.5 kHz for the no-void case and for the void case it is between 5.1 and 6.2 kHz. For a frequency of 6.0 kHz, the wavenumber is k = 28 m^{-1} and the wavelength, λ = 0.23 m. The vertical distance between survey line and void is 0.08 m. Thus, the ratio of the wavelength to the void depth d is equal to λ / d = 2.9 $\approx$ 3.0. This result is in agreement with the numerical simulations, as the optimum wavelength for detection of void is in the range $3 < \lambda/d < 5$ (Tallavo et al., 2009).

5 CONCLUSIONS

This paper presents laboratory and numerical results to evaluate the potential of MASW tests in detection of underground voids from the surface responses. A new methodology is adapted where the total array of receivers

is divided into three sections to understand the interaction of surface waves in presence of anomaly. Analysis of the results using the two-dimensional FFT and the dispersion curves are presented for the two cases, no-void and void. From the numerical simulations it can be observed that void vibrates in the presence of the R-waves which is evident with the reflection in time traces in section 1. Part of the incident energy is attenuated as the waves pass through the void which can be observed in the frequency spectra for section 3.

The experimental sandbox test validates the results obtained from numerical simulations. If the void is present within the 1/3 of the wavelength, energy concentrations on the surface responses above the void are noticeable. To improve these results, the number of accelerometers in the experimental test should be increased to get a better understanding of the interaction of the R-waves in the presence of the void.

ACKNOWLEDGEMENTS

This research is part of a study on non-destructive testing of geomaterials. Support is provided by the Natural Sciences and Engineering Research Council of Canada (NSERC). Support is also provided by Ontario center of Excellence (OCE).

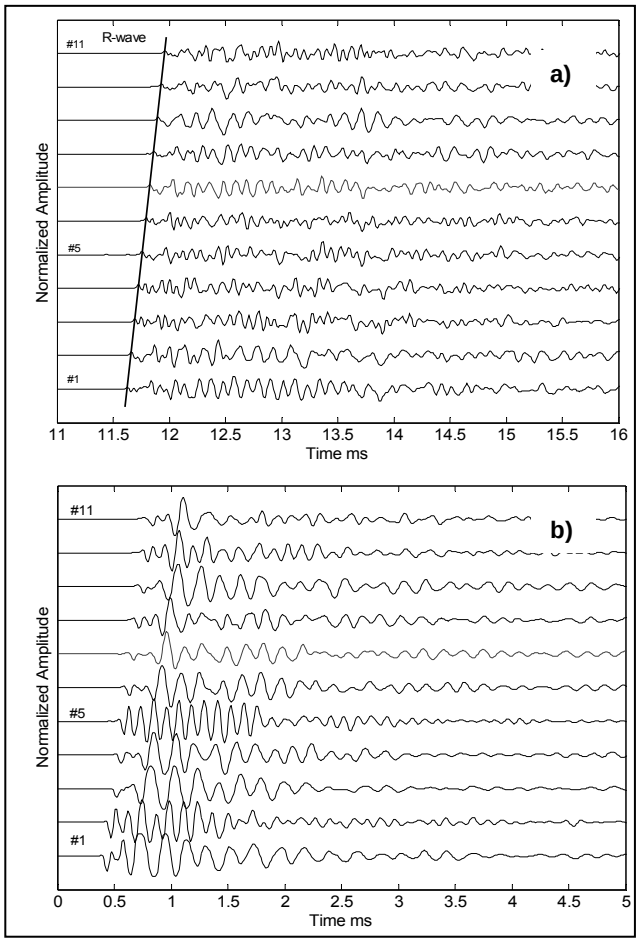

Figure 8: Time domain results for no-void and void cases.

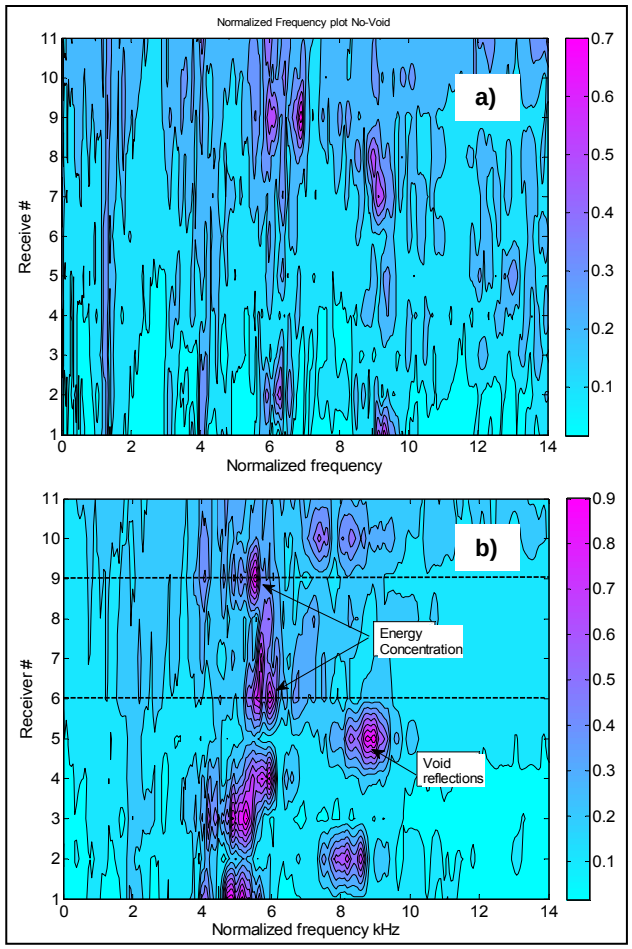

Figure 9: Frequency spectra for a) no-void and b) void cases.

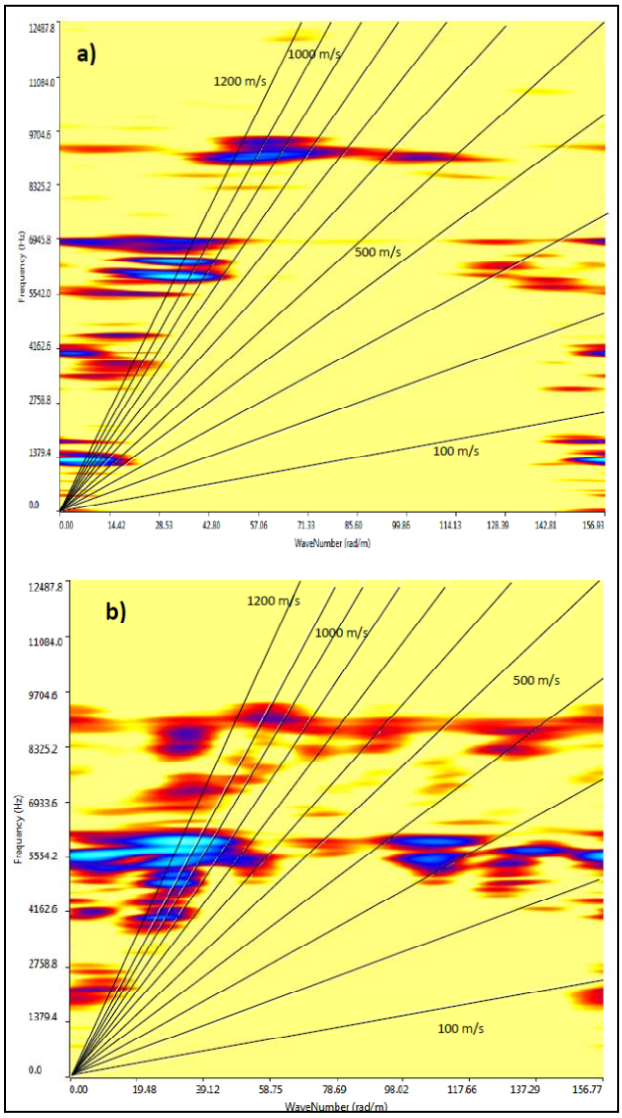

Figure 10: 2D-FFT for the no-void and void cases.

REFERENCES

Ali, H., Nasseri-Moghaddam, A., Cascante, G., Use of numerical simulation for the identification of underground voids. 64th Canadian Geotechnical Conference, Toronto, Canada

Cascante, G., Najjaran, H. and Crespi, P. 2006. Nondestructive Evaluation of Brick Walls – Fuzzy Logic Analysis. *Journal of Infrastructure Systems*, ASCE.

Hiltunen, D. R., and Woods, R. D. 1989. Influence of source and receiver geometry on testing of pavements by the surface waves method. In A. J. Bush III, and Baladi, G. Y. (Eds.), *Nondestructive testing and backcalculation of moduli*, ASTM STP 1026 (pp. 138-154). Philadelphia: American society of testing and materials.

Itasca, 2000. *Flac: fast Lagrangian analysis of continua users guide*. *Minneapolis*, Minnesota: Itasca consulting group Inc.

Kong, F.N., Westerdahl, H., and By, T.L. 1994. Borehole radar tunnel detection at Gjovik, Norway. *Norwegian Geotechnical Institute, Publication 194*, 1-10.

Lamb, H. 1904. On the propagation of tremors over the surface of an elastic solid. *Philos. Trans. r. Soc. London*, Ser. A, 203, 1-42.

Nasseri-Moghaddam, A., Cascante, G., Phillips, C., Hutchinson, D.J. 2007. Effect of underground cavities on Rayleigh waves – Field and numerical experiments. *Journal of Soil Dynamics and Earthquake Engineering*, Issue 27: 300 - 313.

Nasseri-Moghaddam, A., (2006). Study of the effect of lateral inhomogeneities on the propagation of Rayleigh waves in an elastic medium. (Doctoral dissertation). Retrieved from UWSpace (http://hdl.handle.net/10012/781).

Nazarian, S., Stokoe, K. H. 1984. In-situ shear wave velocities from spectral analysis of surface waves, *Proc. of the Eighth World Conf. on Earthquake Engineering*, San Francisco, California, III, July 21 - 28, pp. 31 – 38.

Park, C. B., Miller, R. D., and Xia J. 1999. Multichannel analysis of surface waves. *Geophysics*, 64(3), 800-808.

Phillips, C., Cascante, G., and Hutchinson, J., 2001, Numerical simulation of seismic surface waves: In 54th Canadian Geotechnical Conference, Calgary, Alberta, September, 1538–1545.

Phillips, C., Cascante, G., and Hutchinson, J., 2004, Evaluation of lateral homogeneity with the distance analysis of surface waves: Canadian Geotechnical Journal, 41(2), 212-226.

Stokoe II, K.H., Nazarian, S., Rix, G.J., Sanchez-Salinero, I., Sheu, J.C., and Mok, Y.J. 1988. In-Situ Seismic Testing of Hard-To-Sample Soils by Surface Wave Method. Earthquake Engineering and soil dynamic II - Recent advances in ground-motion evaluation, Von Thun, J.L (ed), Utah, Geotechnical special publication 20: 264-279.

Santamarina, J., Klein, K., and Fam, M. 2001. *Soils and waves*. West Sussex, Eng: John Wiley and Sons Ltd.

Sheu, J.C., Stokoe II, K.H., and Roësset, J.M., 1988, Effect of reflected waves in SASW testing of pavements: Research Record No. 1196, Transportation Research Board, National Research Council, Washington, D.C., 51–61.

Shokouhi, P., Gucunski, N., 2003, Application of wavelet transform in detection of shallow cavities by surface waves: In Proc. Symposium on the Application of Geophysics to Engineering and Environmental Problems, San Antonio, Texas.

SWAN, 2010: Surface wave analysis: Geostudi Astier S.r.l. Livorno, Italy

Tallavo, F., Cascante G., Pandey, M., (2009). Experimental and numerical analysis of MASW tests for detection of buried timber trestles. Soil Dynamics and Earthquake Engineering 29, 91-102

Yang, Y. (2009). Nondestructive evaluation of the depth of cracks in concrete plates using surface waves. Ph.D. thesis, University of Waterloo